Effect of Shape and Depth of Shallow Foundations on Failure Mechanism and Wedge Angle of Sandy Soil

W. Nashaat Abd El Samee(✉)

Civil Engineering Department, Beni-Suef University, Beni-Suef, Egypt
Waelnashat@eng.bsu.edu.eg

Abstract. In the present study, finite element analysis was selected to develop numerical models to study the failure mechanism of sandy soil and the wedge angle. The sandy soil is simulated by a semi-infinite element isotropic homogeneous elastic material. The analysis program consists of five footings with different L/B ratio (Ratio between length and width of footing) ranged between 1 to 8. Each footing was analyzed with different foundation depth. In addition, also different angle of internal friction of sandy soil was taken. It was concluded that, the obtained failure mechanism in the present study is identical with the conventional failure mechanism. In addition, it was concluded also that the wedge angle values obtained in the present study decrease with increasing depth of footing and increasing angle of internal friction of the soil as well as increasing L/B ratio while the wedge angle value of sandy soil obtained from previous theoretical approaches is constant [$\Psi = 45 + (\emptyset/2)$].

Keywords: Failure mechanism · Wedge angle · Sandy soil · Depth of footing Ratio

1 Introduction

The redistribution of stresses within the soil mass, often referred to as arching, has been analyzed using physical and analytical modeling of active and passive zone systems Terzaghi [1]. The movement of an active zone causes a reduction of soil stresses immediately and increase of stresses in the adjacent soil mass.

McManus and Burdon investigated three shallow foundations each 4.25 m wide 4.6 m long consisting of a 100 mm thick slab "on-grade" with two foundation beams 600 mm wide embedded 450 mm constructed in coarse granular material. The tests were supplemented with several, simpler interface sliding tests performed on 2 m wide × 3 m long concrete slabs constructed "on-grade" using one or two layers of polymer damp-proof membranes. Lateral loading of the slab and beam foundations caused a wedge type of failure mechanism with significant passive soil pressures acting against the vertical faces of the foundation beams. The passive soil wedge developing against the trailing beam lifted one side of the structure vertically leaving hollow space beneath the floor slab. For the somewhat narrow structures tested, significant rotations of the structure occurred. A simple method of analysis was developed to give

H. Shehata and B. Das (Eds.): GeoMEast 2018, SUCI, pp. 197–216, 2019.
https://doi.org/10.1007/978-3-030-01923-5_15

predictions for the experimental results while accounting for all of the main parameters. The analysis predicts that lateral load capacity was highly sensitive to the eccentricity of the applied lateral load [2].

Kholdebarin et al. presented a rigid footing model with specified properties and dimensions on a sandy-clay soil with Mohr-coulomb material. This elasto-plastic soil foundation model was analyzed dynamically with finite difference 2D FLAC software under vertical component of ground excitations. Then the soil was improved with cement grouting and analyzed again. Consequently, the vertical stress under a strip footing, due to vertical component of ground accelerations through the underlying soil was plotted. Also the stress distribution and dynamic bearing capacity of natural and soil cemented foundation was presented [3].

Kentaro et al. presented a various types of foundations suitable for a variety of soils and applications as an alternative to conventional flat foundations for the increase of bearing capacity and the savings of materials. The concept of shells was not new in foundation design, considering the construction with inverted brick arch foundation. Various types of foundations with different geometrical shapes have been extensively investigated in the structural design. However, the corresponding studies on the geotechnical design in terms of bearing capacity and deformation are scare. As such the advantages of various of foundations have not yet been clarified in terms of the geotechnical design. The objective of the study was to examine the overall geotechnical performance of various types of foundation on sand using model loading tests and numerical limit analysis. The general superiority of various types of foundations has been revealed by comparing the loading tests with the analysis results [4].

Nguyen and Merifield presented a prediction of the undrained bearing capacity of strip, square, rectangular and circular footings embedded in clay by using finite element analysis. From these analyses, rigorous shape and depth factors have been derived and were compared with previous numerical and empirical solutions in the literature. The bearing capacity behaviour was discussed and the bearing capacity factors were given for various cases involving a range of embedment depths and footing shapes [5].

Conte et al. presented the analyzed of the response of shallow foundations on soils with strain-softening behavior by using finite element approach. In these soils, a progressive failure can occur owing to a reduction of strength with increasing the plastic strains induced by loading. The theoretical approach allows this failure process to be properly simulated by using a non-local elasto – viscoplastic constitutive model in conjunction with a Mohr – Coulomb yield function in which the shear strength parameters were reduced with the accumulated deviatoric plastic strain. Another advantage of the method was that it requires few material parameters as input data, with most of these parameters that can be readily obtained from conventional geotechnical tests. To assess the reliability of the proposed approach, some comparisons with experimental results from physical model tests were presented. A fairly agreement was found between simulated and observed results. The progressive failure process that occurs in a dense sand layer owing to loading was analyzed and the main aspects concerning the associated failure mechanism were highlighted [6].

Zhang et al. presented a method for progressive failure analysis of strain-softening slopes based on the strength reduction method and strain-softening model. The mutation was more pronounced in strain-softening analysis, and the mutation of

displacement at slope crest was taken as critical failure criterion. This method was applied to a cut slope in an industry site. The results were as follows: (i) The thickness of the shear zone considering strain softening behaviour is narrower than that with non-softening analysis. (ii) The failure of slope is the process of the initiation, propagation and connection of potential failure surface. The strength parameters were mobilized to a non-uniform degree while progressive failure occurs in the slope. (ii) The factor of safety increases with the increase of residual shear strain threshold and elastic modulus. The failure mode of slope changes from shallow slip to deep slip. Poisson's ratio and dilation angle have little effect on the results [7].

Qiming and Murad presented some analytical solutions for estimating the ultimate bearing capacity of strip footings on RSFs. A general failure mode for RSFs was first proposed based on previous studies conducted by the authors and test results from literature study. A limit equilibrium stability analysis of RSFs was performed based on the proposed failure mechanism. New bearing capacity formulas, which consider both the confinement and the membrane effects of reinforcements on the increase in ultimate bearing capacity, were then developed for strip footings on RSFs. Several special cases of RSFs were presented and discussed. The proposed model was verified by the experimental data reported in the published literature. The predicted ultimate bearing capacity was in good agreement with the results of model tests reported in the literature. The study showed that the depth of the punching shear failure zone (D_P) depends on the relative strength of the reinforced soil layer and the underlying unreinforced soil layer [8].

El-Samny et al. presented the effect of footing shape and size on the wedge angle. The wedge angle of cohesionless soil at surface with and without surcharge has been determined in field for graded sand samples. The tests have been conducted in field by using the plate load test. The relationships between the wedge angle and the angle of internal friction have been obtained. An empirical formula to determine the wedge angle for circular, square and rectangular plates at different depths has been presented. The relationships between the wedge angle and the ratio (D/B) of footing depth and width have been also obtained [9].

Acharyya and Dey presented the effect of foundation placed on a slope on the ultimate bearing capacity by its vicinity to the slope face, which offers substantially lesser passive resistance as compared to a footing resting on a semi-infinite medium. Conventional bearing capacity theories fail to address the behavior of such foundations. However, deformation along the slope plays a major role in governing the failure of such foundations, thus requiring a coupled stress-deformation based failure analysis. With the aid of 3-D finite element modelling, employing coupled stress deformation analysis. Addresses the failure mechanism and the bearing capacity (q_u) of a square footing located on a dry cohesionless slope. The effect of various parameters, namely the angle of internal friction of soil, setback distance, slope inclination, footing width and the depth of embedment of the footing, have been investigated. Variations parameters were found to noticeably alter the bearing capacity estimate and the observed failure mechanism. The unit weight and modulus of elasticity of the soil material was found to have negligible effect on the bearing capacity [10].

The main aim of the present study is to determine, the effect of shape and depth of shallow foundations on wedge angle and failure mechanism of soil. In addition,

determine, the effect of angle of internal friction of the soil as well as increasing L/B ratio on wedge angle and failure mechanism of soil.

2 Failure Mechanism

The true theoretical failure mechanism is determined using theory of plasticity concepts and is illustrated conceptually in Fig. 1.

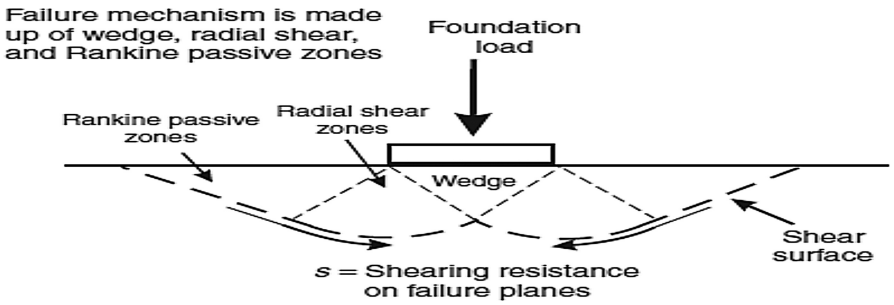

Fig. 1. Failure mechanism for bearing capacity [11].

Where:

$$\Psi = \text{wedge angle} = 45 + \Phi/2 \quad \alpha = 45 - \Phi/2 \quad \text{B : Width of footing.}$$

Prandtl [11] developed an equation based on his study of penetration of long hard metal puncher into softer materials for computing the ultimate bearing capacity. The mechanisms of failure of soil under plastic equilibrium are:

i. Failure occurs along definite slip surfaces and symmetrical with respect to the centerline of the puncher or footing in the case of soil for symmetrical vertical loading.
ii. Under ultimate, load Q_{ult} acting on the footing of width B as shown in Fig. 2, a triangular wedge of soil abc is formed below the footing and pushed down as a rigid body. The stresses acting on abc will be in active stage.

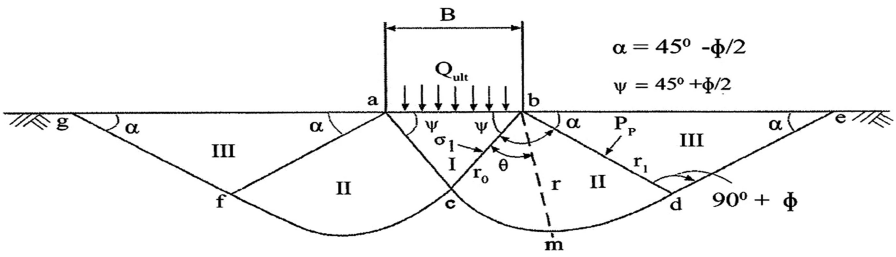

Fig. 2. Failure surface [11].

iii. Due to gradual downward push of the wedge abc, the soil mass on its left and right will be pushed outward and upward. The failure takes place along the slip surfaces bcde and acfg. These surfaces comprise triangular wedges bde and afg, and sectors bcd and acf.
iv. The mass of soil will be in a plastic state above the failure surface gfcde and in elastic state below the surface.
v. The failure surfaces can be divided into three Zones I to III. Zone I will be in active state, Zone II in radial shear and Zone III in plastic state.
vi. The lower boundaries of zone II are parts of logarithmic spirals with their poles coinciding with the corresponding edge of the footing. The straight lines de and fg are tangential to spirals at points d and f respectively and meet the horizontal surface.

Terzaghi studied change in the properties of soil behavior beneath and around the foundation [12, 13]. It is based ultimate bearing capacity theory for strip footing. Failure mechanism and width footing explain this theory. Later on, Meyerhof and Hansen (1963) expanded Terzaghi theory. Terzaghi in (1943) gave a general bearing capacity theory for a strip foundation. For the first time, he developed his theory by incorporating weight of failure wedge in the analysis. Terzaghi considered a continuous footing of width B placed at a depth of D below the ground surface as shown in Fig. 2. The soil is assumed to fail along the surface (aedcgfb). The failure surface consists of 5 zones. The Zone I, abc is an elastic zone. Zone II, which comprises wedges beg and acd is the zone of radial shear. The wedges bfg and ade comprise Zone III and are known as passive Rankine's zone and will be in a plastic state. When the footing is loaded the wedge abc sinks into the ground as an integral part of the footing and remains in the elastic state due to the cohesion and adhesion between the base of the footing and the soil. The straight boundaries ac and bc of this zone are inclined at an angle with the base of the footing. In Zones II and III, shear patterns develop. Zone II, the zone of radial shear constitutes a set of radial lines emerging from the outer edges b and a of the footing.

3 Finite Element Analysis

Finite element method was selected in the present study to develop numerical models to study the failure angle in soil (wedge angle). The finite element analysis was performed using two finite element software (Optum & Limitstate) [14, 15], limit analysis was performed in this study including upper and lower bound. A semi-infinite element isotropic homogeneous elastic material simulates the soil and the material model used is Mohr-Coulomb, while the concrete simulated as rigid material.

3.1 Numerical Program

The analysis program consists of five footings including square footing and rectangular footings with L/B ratio (Ratio between length and width of footing) ranged between 1 to 4 and 8. Each footing was analyzed with foundation depth ranged between 0.0 B,

0.10 B. 0.15 B, 0.25 B, 0.50 B and 1.0 B. The angle of internal friction of sandy soil used was also ranged between 30°, 35°, 38° and 40°. The analysis program is shown in Table 1. The soil is simulated by a semi-infinite element isotropic homogeneous elastic material. The type of soil is sand. The used soil properties are listed in Table 2.

Table 1. Investigated cases of study by numerical analysis program.

Footing shape	L/B ratio	Angle of internal friction (Ø)	Depth of foundation (D_f)
Square footing (B * B)	1	30°, 35°, 38° and 40°	0.00 B
			0.10 B
			0.15 B
			0.25 B
			0.50 B
			1.00 B
Rectangular footing (L * B)	2	30°, 35°, 38° and 40°	0.00 B
			0.10 B
			0.15 B
			0.25 B
			0.50 B
			1.00 B
Rectangular footing (L * B)	3	30°, 35°, 38° and 40°	0.00 B
			0.10 B
			0.15 B
			0.25 B
			0.50 B
			1.00 B
Rectangular footing (L * B)	4	30°, 35°, 38° and 40°	0.00 B
			0.10 B
			0.15 B
			0.25 B
			0.50 B
			1.00 B
Strip footing (L * B)	8	30°, 35°, 38° and 40°	0.00 B
			0.10 B
			0.15 B
			0.25 B
			0.50 B
			1.00 B

Where:
D_f: Depth of footing. L: Length of footing. B: Width of footing.
L/B: Ratio between length and width of footing.

Table 2. Soil properties.

Parameters	Soil
Material model	Mohr - Coulomb
Type of material	Fine to med sand
Thickness (m)	10
Unit weight, γ (kN/m^3)	17.5
Young's modulus, E_s (kN/m^2)	15000
Poisson's ratio, υ	0.25
Friction angle, Ø (deg)	30, 35, 38 and 40
Dilatancy angle, ¥ (deg)	0, 5, 8 and 10

3.2 Failure Mechanisms by Finite Element

The failure mechanism in the soil beneath large footings is observed internally thus movement of soil around the foundation is seen (the passive zone is not distinguished clearly). This mechanism is identical from what Terzaghi has proposed. Increasing lateral pressure (confining) the ground located under the footing will increase the pressure bearing in this region. According to the conventional failure mechanism, stress is distributed in the soil beneath and around the footing, so, the stress penetration depth decreases (formation of stress bubbles). According to the proposed models in the present study, in order to predict and interpret the results obtained from numerical analysis, the effect of shape and depth of shallow foundations on wedge angle and failure mechanism of soil have been obtained. Figures 3, 4, 5, 6, 7, 8, 9, 10 and 11 show examples of failure mechanism for the modeled footings.

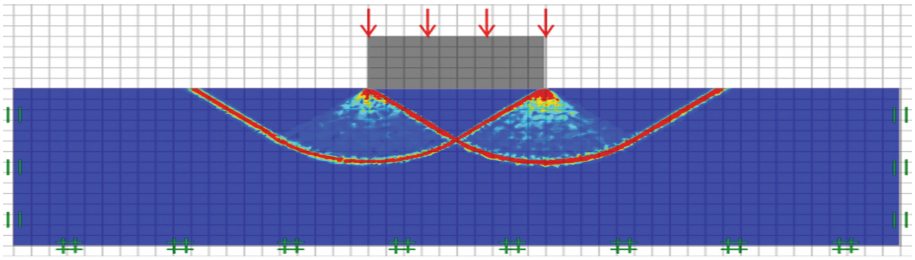

(3-a) Failure mechanism of square footing L/B = 1.00.

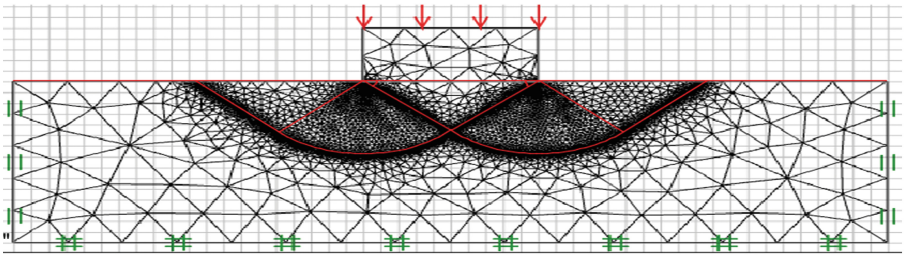

(3-b) Failure mechanism (deformed mesh) of square footing L/B = 1.00.

Fig. 3. Failure mechanism of square footing L/B = 1.00, at Ø = 30° and at D_f = 0.00 B.

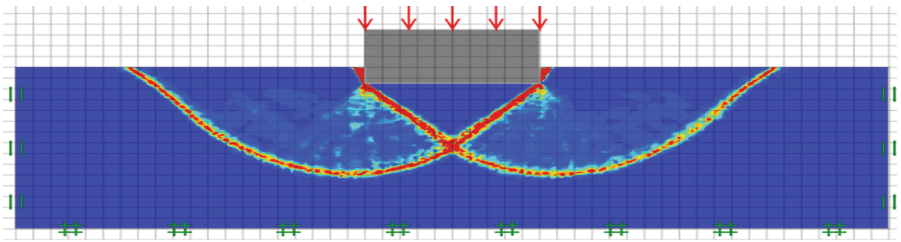

(4-a) Failure mechanism of square footing L/B = 1.00.

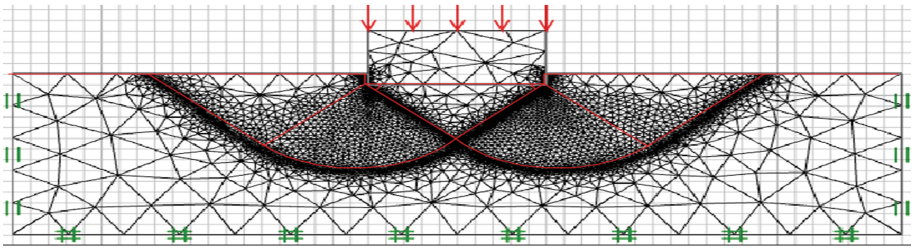

(4-b) Failure mechanism (deformed mesh) of square footing L/B = 1.00.

Fig. 4. Failure mechanism of square footing L/B = 1.00, at Ø = 30° and at Df = 0.25 B.

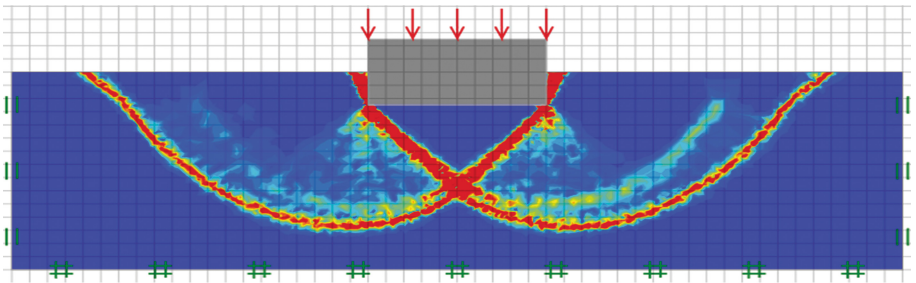

(5-a) Failure mechanism of square footing L/B = 1.00.

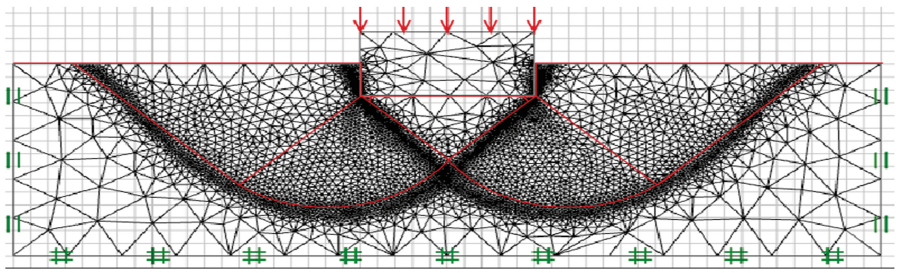

(5-b) Failure mechanism (deformed mesh) of square footing L/B = 1.00.

Fig. 5. Failure mechanism of square footing L/B = 1.00, at Ø = 30° and at D_f = 0.50 B.

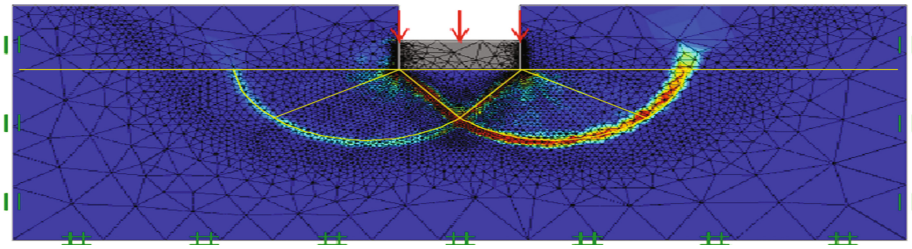

Fig. 6. Failure mechanism of square footing L/B = 1.00, at Ø = 30° and D_f = 1.00 B.

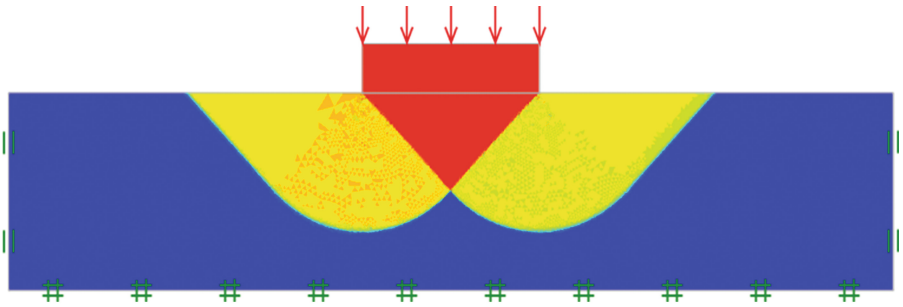

(7-a) Failure mechanism of rectangular footing L/B = 2.00.

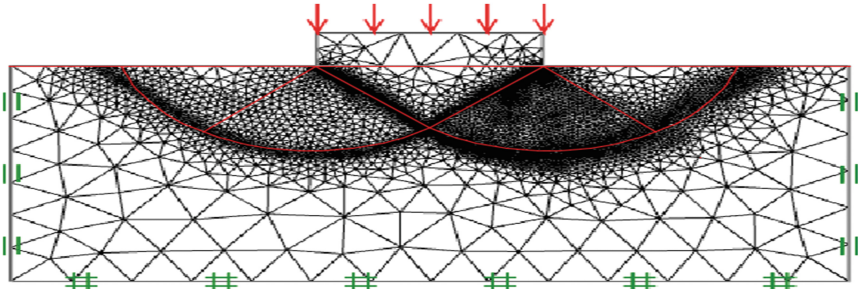

(7-b) Failure mechanism (deformed mesh) of rectangular footing L/B = 2.00.

Fig. 7. Failure mechanism of rectangular footing L/B = 2.00, at Ø = 30° and D_f = 0.00 B.

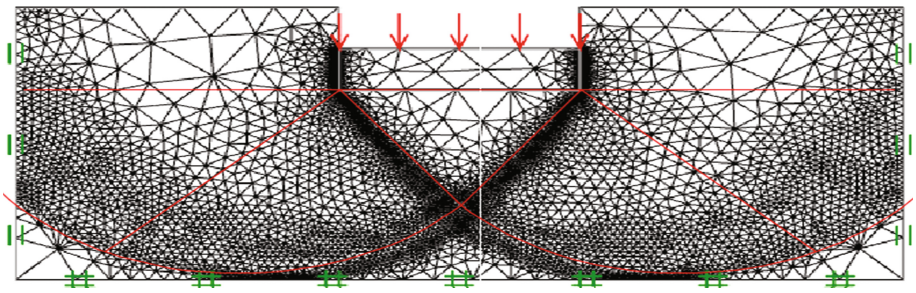

Fig. 8. Failure mechanism of rectangular footing L/B = 2.00, at Ø = 30° and D_f = 0.50 B.

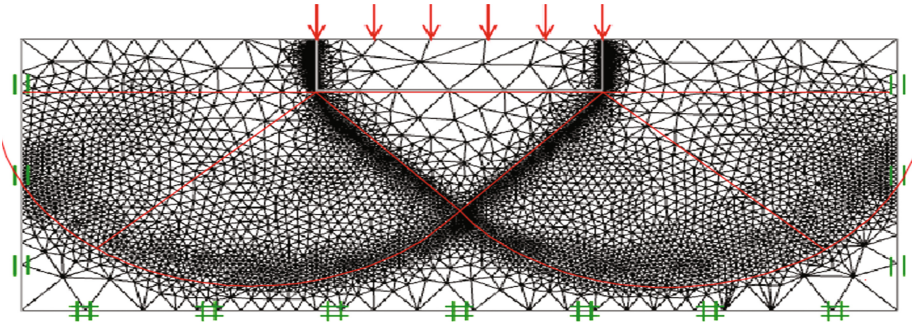

Fig. 9. Failure mechanism of rectangular footing L/B = 3.00, at Ø = 30° and D_f = 0.25 B.

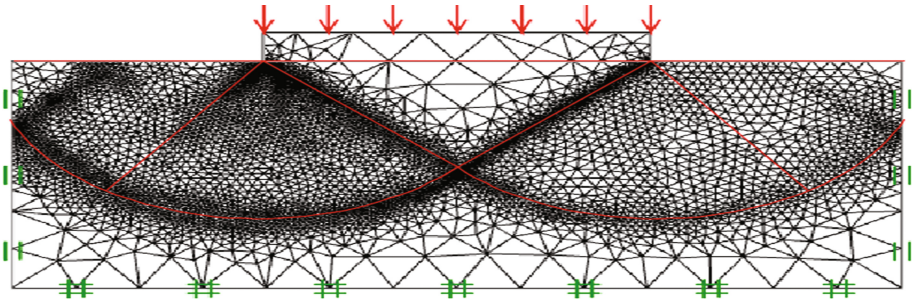

Fig. 10. Failure mechanism of rectangular footing L/B = 4.00, at Ø = 30° and D_f = 0.00 B.

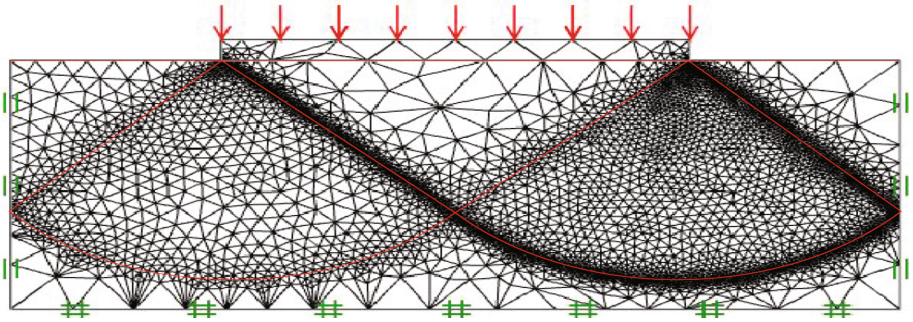

Fig. 11. Failure mechanism of strip footing L/B = 8.00, at Ø = 30° and D_f = 0.00 B

From these figures it can be noticed that, the obtained failure mechanism in the present study is identical with the conventional failure mechanism.

4 Finite Element Results

The obtained results from the numerical analysis are described as follows:

4.1 Determination of Failure Angle (Wedge Angle)

The failure angle (wedge angle) in soil has been obtained using finite element models through locating the points of deformation along the axis of the triangle of failure which is the active zone, then by drawing a line intersecting these points it results in a triangle shape. By knowing the triangle axis lengths, the angle between the triangle sides are then determined as shown in Fig. 12.

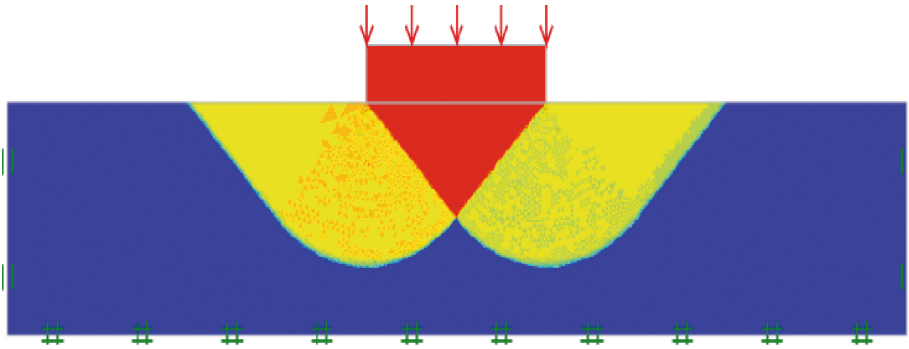

(12-a) Failure mechanism of rectangular footing L/B.

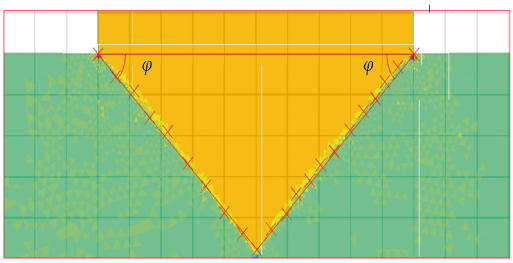

(12-b) (wedge angle of failure mechanism for rectangular footing L/B

Fig. 12. Determination of failure angle (wedge angle).

4.2 Effect of Ratio L/B on Failure (Wedge) Angle of Soil

The values of failure (wedge) angle of sandy soil have been obtained by the numerical analysis and compared with values of wedge angle obtained by theoretical approaches using Terzaghi and Meyerhof are presented in Table 3. A comparison between the values of wedge angle of sandy soil with the ratio L/B (shape of shallow foundation) is presented in Figs. 13, 14, 15 and 16.

Table 3. The obtained values of wedge angle by numerical analysis program and compared with values of wedge angle obtained by theoretical approaches using Terzaghi and Meyerhof at Ø = 30°, 35°, 38° and 40°.

Footing shape	L/B ratio	Depth of foundation (D_f)	Obtained values of wedge angle (Ψ) by finite element				Terzaghi and Meyerhof Ψ = 45 + (Ø/2)			
			(Ø) = 30°	(Ø) = 35°	(Ø) = 38°	(Ø) = 40°	(Ø) = 30°	(Ø) = 35°	Ø) = 40°	(Ø) = 45°
Square footing (B * B)	1	0.00 B	48.35	47.38	46.67	46.44	60.00	62.50	64.00	65.00
		0.10 B	47.95	46.99	46.29	46.05				
		0.15 B	47.60	46.65	45.95	45.72				
		0.25 B	47.20	46.26	45.56	45.33				
		0.50 B	46.30	45.37	44.69	44.47				
		1.00 B	45.80	44.88	44.21	43.99				
Rectangular footing (L * B)	2	0.00 B	47.60	46.65	45.95	45.72				
		0.10 B	47.25	46.31	45.61	45.38				
		0.15 B	46.85	45.91	45.22	44.99				
		0.25 B	46.50	45.57	44.89	44.66				
		0.50 B	45.50	44.59	43.92	43.70				
		1.00 B	44.70	43.81	43.15	42.93				
Rectangular footing (L * B)	3	0.00 B	46.80	45.85	45.16	44.99				
		0.10 B	46.20	45.30	44.62	44.47				
		0.15 B	45.85	44.90	44.23	44.03				
		0.25 B	45.55	44.50	43.83	43.65				
		0.50 B	44.65	43.81	43.15	42.83				
		1.00 B	43.65	42.75	42.11	41.95				
Rectangular footing (L * B)	4	0.00 B	45.80	44.88	44.21	43.99				
		0.10 B	45.35	44.44	43.78	43.55				
		0.15 B	44.90	44.00	43.34	43.12				

(*continued*)

Table 3. (*continued*)

Footing shape	L/B ratio	Depth of foundation (D_f)	Obtained values of wedge angle (Ψ) by finite element				Terzaghi and Meyerhof Ψ = 45 + (Ø/2)			
			(Ø) = 30°	(Ø) = 35°	(Ø) = 38°	(Ø) = 40°	(Ø) = 30°	(Ø) = 35°	Ø) = 40°	(Ø) = 45°
		0.25 B	44.68	43.66	43.00	42.79				
		0.50 B	43.78	42.92	42.28	42.07				
		1.00 B	42.55	41.70	41.07	40.87				
Strip footing (L * B)	8	0.00 B	44.90	44.00	43.34	43.12				
		0.10 B	44.45	43.56	42.91	42.69				
		0.15 B	44.10	43.22	42.57	42.35				
		0.25 B	43.80	42.92	42.28	42.07				
		0.50 B	42.90	42.04	41.41	41.20				
		1.00 B	41.30	40.47	39.87	39.66				

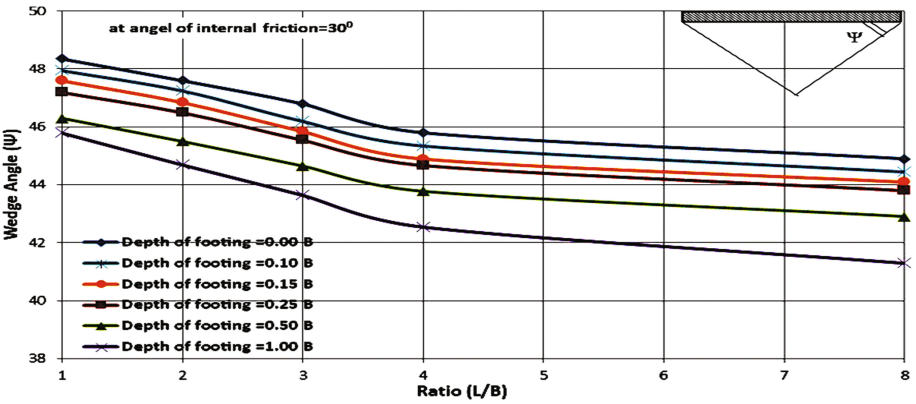

Fig. 13. Comparison of the values of wedge angle and the ratio L/B at different of depth of footing (D_f) and at angle of internal friction (Ø) = 30°.

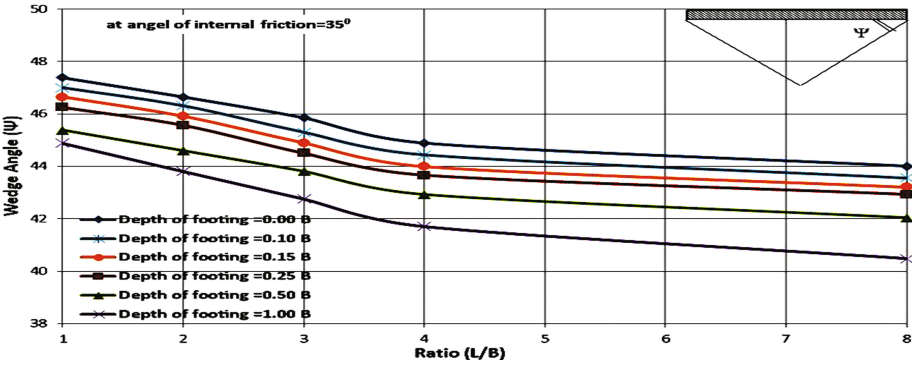

Fig. 14. Comparison of the values of wedge angle and the ratio L/B at different of depth of footing (D_f) and at angle of internal friction (Ø) = 35°.

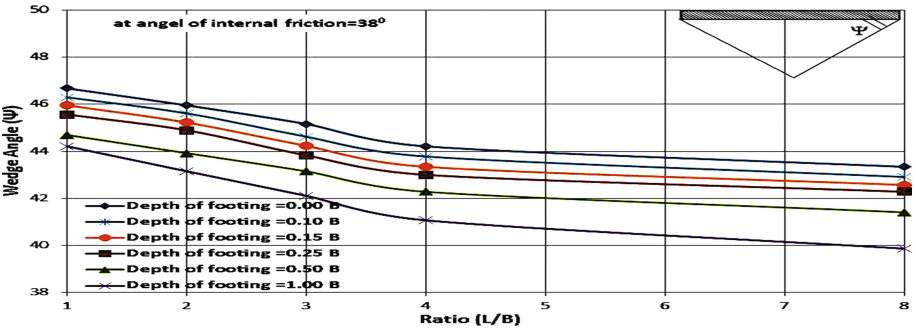

Fig. 15. Comparison of the values of wedge angle and the ratio L/B at different depths of footing (D_f) and at angle of internal friction (Ø) = 38°.

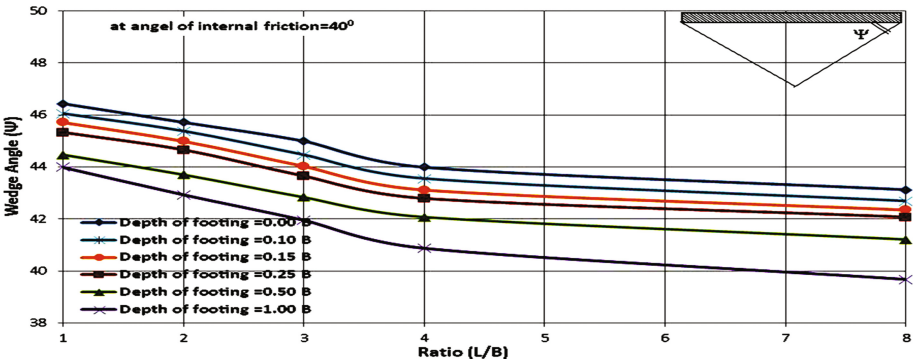

Fig. 16. Comparison of the values of wedge angle and the ratio L/B at different of depth of footing (D_f) and at angle of internal friction (Ø) = 40°.

4.3 Effect of Angle of Internal Friction on Wedge Angle of Soil

A comparison between the values of wedge angle of sandy soil with the angle of internal friction is presented Figs. 17, 18, 19, 20, 21 and 22. show the relationships between angle of internal friction of sandy soil and the wedge angle under different shape of shallow foundation (ratio L/B) for different depths of footings.

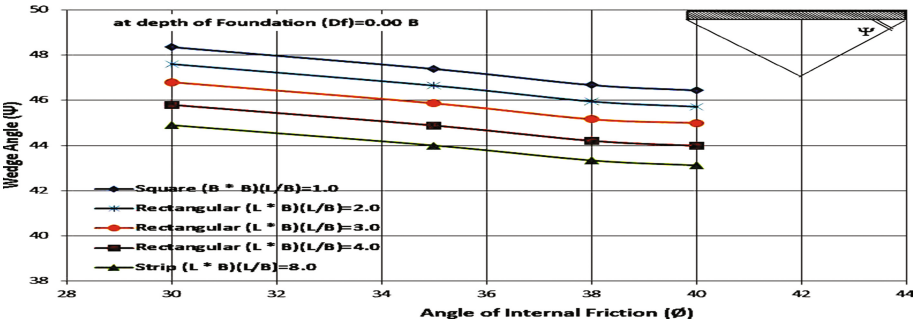

Fig. 17. Relationship between angle of internal friction (Ø) and wedge angle (ψ) at surface under different shapes of footings.

From Table 3 and Figs. 13, 14, 15, 16, 17, 18, 19, 20, 21 and 22, it can be concluded that the wedge angle values of sandy soil decrease with increasing depth of footing and increasing of angle of internal friction of the soil as well as increasing L/B ratio (Ratio between length and width of footing).

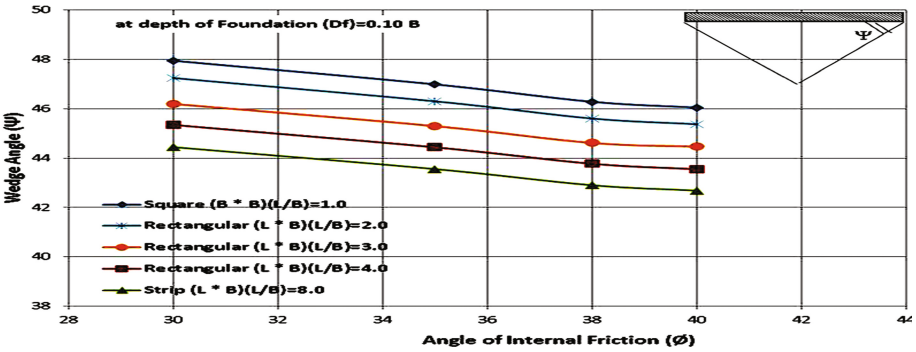

Fig. 18. Relationship between angle of internal friction (Ø) and wedge angle (ψ) at surface under different shapes of footings.

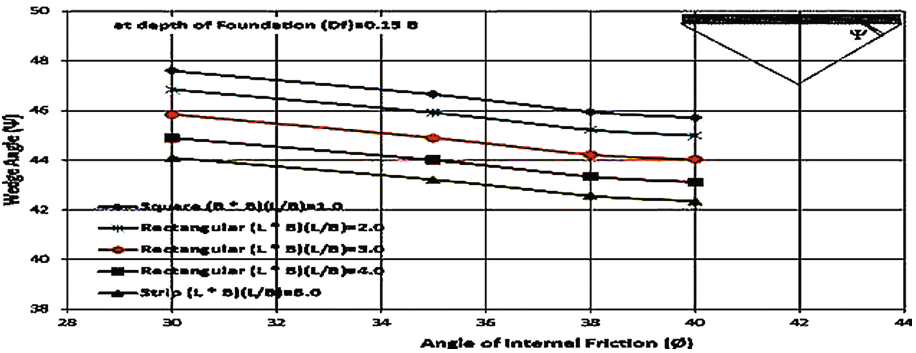

Fig. 19. Relationship between angle of internal friction (Ø) and wedge angle (ψ) at surface under different shapes of footings.

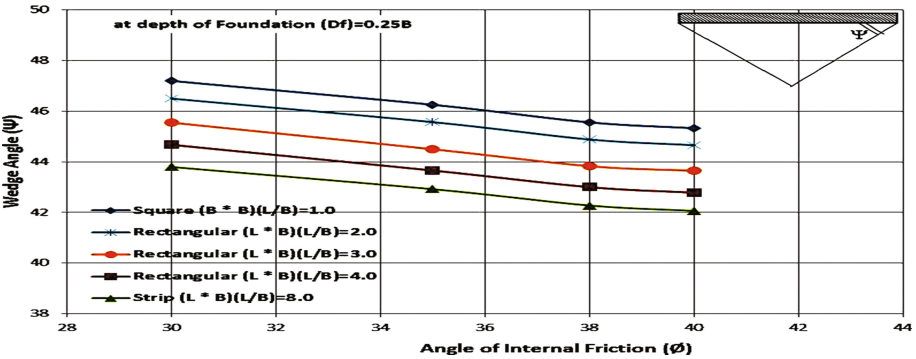

Fig. 20. Relationship between angle of internal friction (Ø) and wedge angle (ψ) at surface under different shapes of footings.

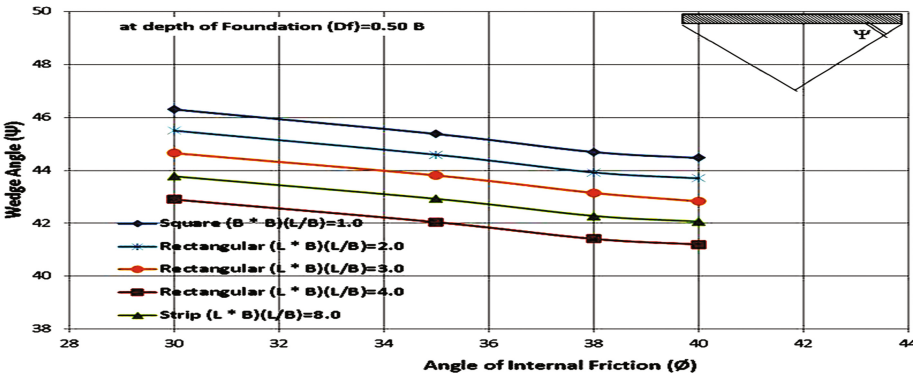

Fig. 21. Relationship between angle of internal friction (Ø) and wedge angle (ψ) at surface under different shapes of footings.

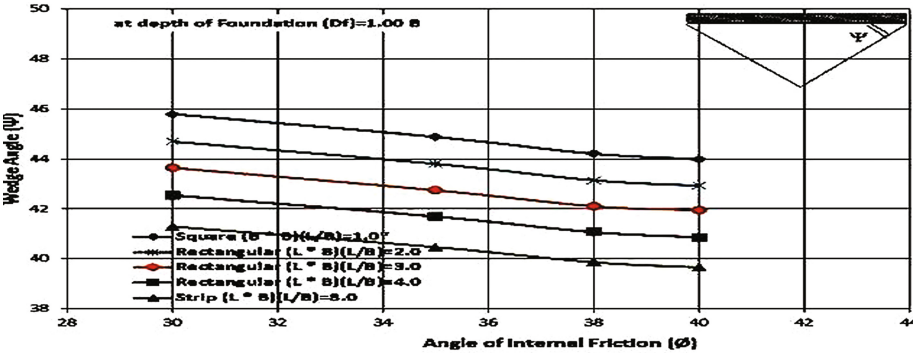

Fig. 22. Relationship between angle of internal friction (Ø) and wedge angle (ψ) at surface under different shapes of footings.

4.4 Comparison Between Values of Wedge Angle Obtained by Numerical Analysis and Theoretical Approaches

A comparison between values of wedge angle obtained by the present numerical analysis and theoretical approaches is presented in Figs. 23, 24, 25, 26, 27 and 28.

From these figures, it can be concluded that the wedge angle values obtained in the present study decrease with increasing depth of footing and increasing angle of internal friction of the soil as well as increasing L/B ratio while the wedge angle value of sandy soil obtained from previous theoretical approaches is constant [$\Psi = 45 + (\text{Ø}/2)$].

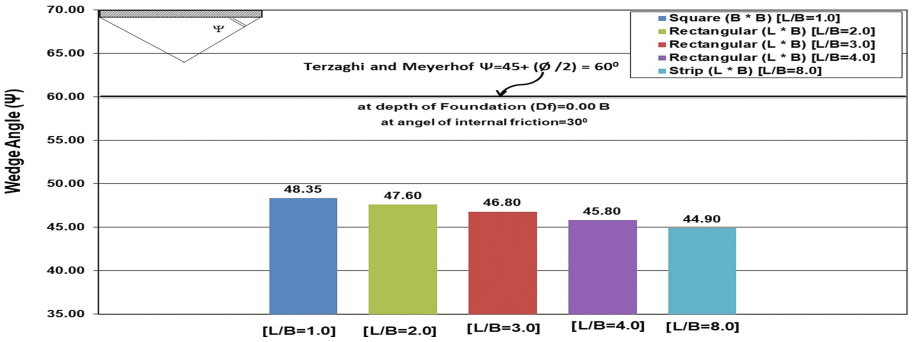

Fig. 23. Comparison between values of wedge angle have been obtained by numerical analysis and by using Terzaghi and Meyerhof at surface (0.00 B).

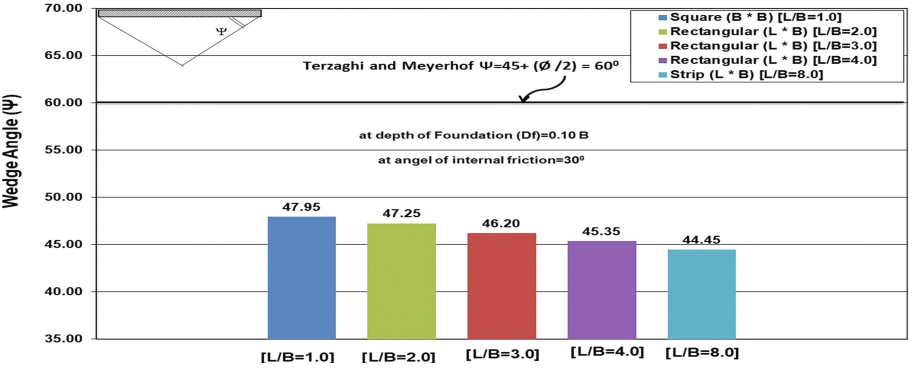

Fig. 24. Comparison between values of wedge angle have been obtained by numerical analysis and by using Terzaghi and Meyerhof at depth of footing = (0.10 B).

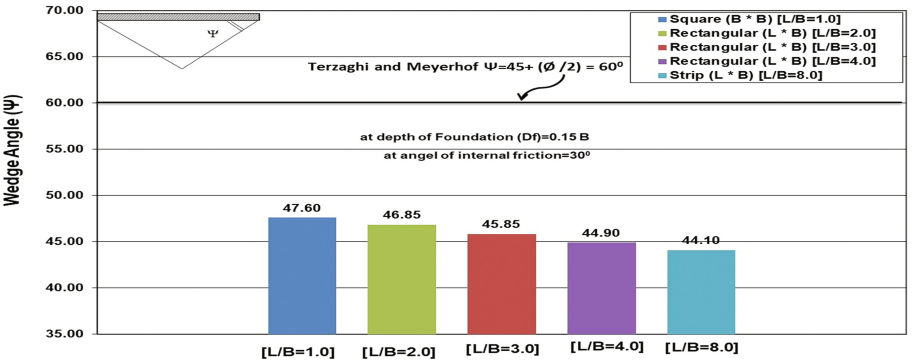

Fig. 25. Comparison between values of wedge angle have been obtained by numerical analysis and by using Terzaghi and Meyerhof at depth of footing = (0.15 B).

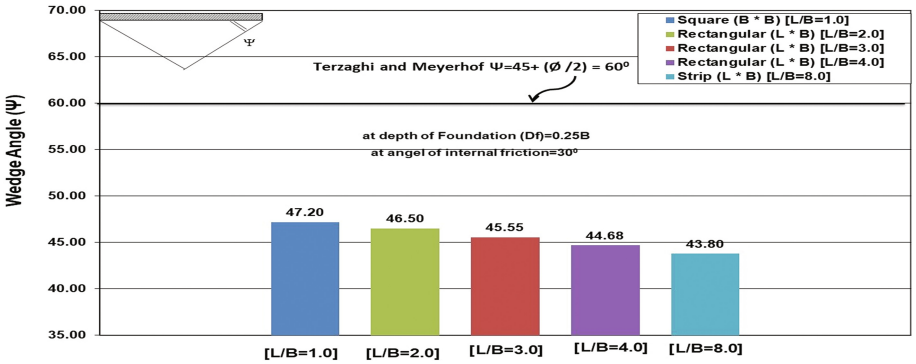

Fig. 26. Comparison between values of wedge angle have been obtained by numerical analysis and by using Terzaghi and Meyerhof at depth of footing = (0.25 B).

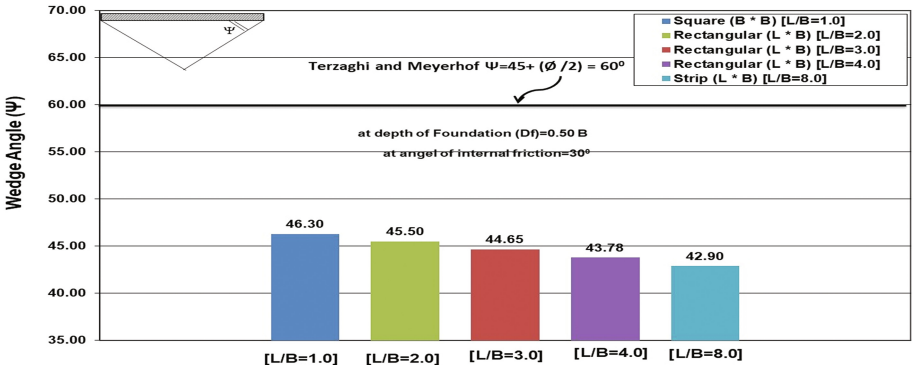

Fig. 27. Comparison between values of wedge angle have been obtained by numerical analysis and by using Terzaghi and Meyerhof at depth of footing = (0.50 B).

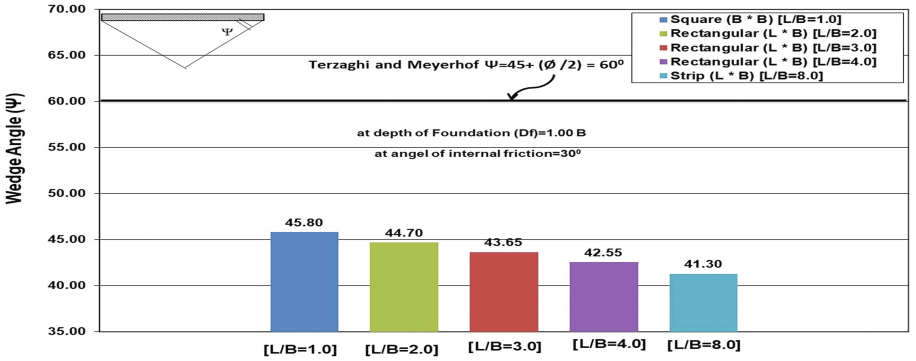

Fig. 28. Comparison between values of wedge angle have been obtained by numerical analysis and by using Terzaghi and Meyerhof at depth of footing = (1.00 B).

5 Conclusions

From the present study results, the following conclusions are obtained:

i. The obtained failure mechanism in the present study is identical with the conventional failure mechanism.
ii. The wedge angle values obtained in the present study decrease with increasing depth of footing and increasing angle of internal friction of the soil as well as increasing L/B ratio while the wedge angle value of sandy soil obtained from previous theoretical approaches is constant [$\Psi = 45 + (\text{Ø}/2)$].

References

1. Terzaghi, K.: The actual factor of safety of foundations. Struct. Engr. **13**, 126–160 (1935)
2. McManus, K.J., Burdon, N.R.R.: Lateral resistance of shallow foundations. In: Conference Paper No. 6.03.01. University of Canterbury, Department of Civil Engineering, NZSEE 2001 (2001)
3. Kholdebarin, A.R., Massumi, A., Davoodi, M.: Influence of soil improvement on seismic bearing capacity of shallow foundation. In: The 14th World Conference on Earthquake Engineering, Beijing, China, 12–17 October 2008
4. Yamamoto, K., Lyamin, A.V., Abbo, A.J.: Bearing capacity and failure mechanism of different types of foundations on sand. Soil Found. **49**(2), 305–314 (2009)
5. Nguyen, V.Q., Merifield, R.S.: Two-and three-dimensional undrained bearing capacity of embedded footings. Aust. Geomech. **47**(2), 25–40 (2012)
6. Conte, E., Donato, A., Troncone, A.: Progressive failure analysis of shallow foundations on soils with strain-softening behavior. Comput. Geotech. **54**(2013), 117–124 (2013)
7. Zhang, K., Cao, P., Bao, R.: Progressive failure analysis of slope with strain-softening behaviour based on strength reduction method. J. Zhejiang Univ.-Sci. (Appl. Phys. Eng.) **14** (2), 101–109 (2013). ISSN: 1673-565X (Print), ISSN: 1862-1775 (Online), www.zju.edu.cn/jzus, www.springerlink.com, E-mail: jzus@zju.edu.cn
8. Chenn, Q., Abu-Farsakh, M.: Ultimate bearing capacity analysis of strip footings on reinforced soil foundation. Soils Found. J. **55**, 74–85 (2015). www.sciencedirect.com
9. El-Samny, M.K., Elsideek, M.B., Abd Elsamee, W.N.: The impact of forms and sizes footings on the corner of collapse triangle in sandy soil. Int. J. Adv. Res. Comput. Sci. Technol. (IJARCST 2015) **3**(2), 76–85 (2013). ISSN: 2347-8446 (Online) ISSN: 2347-9817 (Print) © 2013, IJARCST All Rights Reserved, April–June 2015. www.ijarcst.com
10. Acharyya, R., Dey, A.: Finite element investigation of the bearing capacity of square footings resting on sloping ground. INAE Lett. (2017) **2**, 97–105 (2017). https://doi.org/10.1007/s41403-017-0028-6
11. Prandtl, L. Über die härte plastischer körper. Nachr. Ges. Wiss. Goettingen, Math.-Phys. Kl., pp. 74–85 (1920)
12. Terzaghi, K.: Theoretical Soil Mechanics, p. 528. Wiley, New York (1943). ISBN: 978-0-471-85305-3
13. Meyerhof, G.G.: Some recent research on the bearing capacity of foundations. Can. Geotech. J. **1**, 224–229 (1963)
14. Optum G2, v2, 2018.02.27 (www.optum.com)
15. Limitstate GEO v3.4 (www.limistate.com)